

Relic neutralinos in a best-fitted MSSM

A. Bottino^{a,b}*, G. Mignola^{c,b}, M. Olechowski^{a,b}† and S. Scopel^{d,e}

^a *Dipartimento di Fisica Teorica, Università di Torino, Via P. Giuria 1, 10125 Turin, Italy*

^b *INFN, Sezione di Torino, Via P. Giuria 1, 10125 Turin, Italy*

^c *Theoretical Physics Division, CERN, CH-1211 Geneva 23, Switzerland*

^d *Dipartimento di Fisica, Università di Genova, Via Dodecaneso 33, 16146 Genoa, Italy*

^e *INFN, Sezione di Genova, Via Dodecaneso 33, 16146 Genoa, Italy*

Abstract

We examine the properties of relic neutralinos in the regions of the parameter space selected by recent fits to all the electroweak observables within the Minimal Supersymmetric Standard Model. We discuss the relic neutralino cosmic abundance and the direct detection rates for these most likely supersymmetric configurations. We employ the relevant experimental bounds to constrain the set of the best-fit configurations and discuss the discovery potential of the direct search for relic neutralinos.

CERN-TH 96-103
April 1996

*E-mail: bottino@to.infn.it, mignola@vxcern.cern.ch, olechowski@to.infn.it, scopel@ge.infn.it

†On leave of absence from the Institute of Theoretical Physics, Warsaw University, Poland.

I. INTRODUCTION

The Minimal Supersymmetric extension of the Standard Model (MSSM) has been analysed by many authors in a variety of different theoretical schemes. These various scenarios range from the most model-independent one, whose parameters at the M_Z scale are constrained only by experimental bounds, with no assumptions about properties at higher scales, to more sophisticated ones, where the quantities at M_Z are derived from a few parameters at the Grand Unification (GU) scale ($M_{GUT} = O(10^{16})$ GeV), with the further requirement that the ElectroWeak Symmetry Breaking (EWSB) occurs radiatively.

The specific hypotheses that are assumed at M_{GUT} are very crucial for the phenomenological properties of the supersymmetric particles at the M_Z scale. One often assumes that the soft-breaking mass parameters (scalar masses, gaugino masses and trilinear couplings) unify at M_{GUT} as well as the gauge couplings and the b - τ Yukawa couplings. It is worth remarking that relaxing some of these unification requirements may modify substantially the supersymmetric phenomenology [1,2]. The implications of a relaxation of the soft scalar mass unification at M_{GUT} on the properties of relic neutralinos (relic abundance and detection rates) are discussed in Refs. [3,4].

Unfortunately, at present we do not have enough information from experimental data on which would be the most reliable supersymmetric scheme. In view of this situation, particularly attractive is the approach developed recently, where the parameters of the MSSM at M_Z are considered as independent variables in a global fit to the electroweak data without any further theoretical assumption [5–10]. The fit to all the available experimental data singles out some specific regions of the supersymmetric parameter space as the most likely ones. Furthermore, this analysis, which is performed at the M_Z scale, may provide useful insight into the most plausible theoretical scenario at the M_{GUT} scale.

In the present note we examine which phenomenological consequences this global fit entails, within the MSSM, for relic neutralinos. For the most likely domains of the parameter space we discuss the features of the relevant neutralino relic abundance and of the event rates for the direct search.

II. χ^2 ANALYSIS WITHIN THE MSSM

In the global fits of the electroweak data performed in the framework of the MSSM a key role is played by the ratio $R_b \equiv \Gamma(Z \rightarrow \bar{b}b)/\Gamma(Z \rightarrow \text{hadrons})$ whose experimental value shows a discrepancy (at the level of 3.2 standard deviations) with respect to the value predicted by the Standard Model (SM). In fact, the experimental result $R_b^{exp} = 0.2211 \pm 0.0016$ [11] has to be confronted to the SM prediction $R_b^{SM} = 0.2160$ for $m_t = 170$ GeV (or $R_b^{SM} = 0.2158$ for $m_t = 180$ GeV). The MSSM may resolve this disagreement (at least partially), since the contributions of some supersymmetric loop diagrams add positively to the SM prediction [12,6–10]. More specifically, substantial supersymmetric contributions occur in two regions of the supersymmetric parameter space: (i) for small $\tan\beta$, when both the chargino and one top squark are light, and (ii) for large $\tan\beta$, when the CP-odd Higgs boson A is light and/or both the chargino and one top squark are light (also light neutralino and bottom squark would help in increasing R_b). As usual $\tan\beta$ is defined as $\tan\beta = v_2/v_1$, where v_1 and v_2 are

the vacuum expectation values of the Higgs doublets H_1 and H_2 , which give masses to the down-type and up-type quarks, respectively.

Thus, including R_b in the overall set of the EW data makes the χ^2 fit within the MSSM superior to the one within the SM. At the same time, the experimental range for R_b , combined with other important inputs ($b \rightarrow s\gamma$, bound on m_h , etc.) is very instrumental in placing stringent bounds on the supersymmetric parameter space. Due to the properties recalled above, it is natural that the best fit of the electroweak data within the MSSM automatically selects either (i) very small values of $\tan\beta$ (i.e. close to the quasi-IR fixed point for a given value of m_t) or (ii) very large values of $\tan\beta$ (i.e. of order m_t/m_b) with appropriate ranges for the masses of A boson, chargino, top squark, neutralino and bottom squark [7–10].

It is worth recalling that the fit within the MSSM also has the advantage of providing a value for the strong coupling constant $\alpha_s(M_Z)$, which is lower than the one found with a SM fit, and in agreement with the measurements of α_s at $q^2 \ll M_Z^2$ [13–15]. Actually, this is expected, since lower values of $\alpha_s(M_Z)$ and additional contributions to the Z hadronic width are related properties [7–9,16].

A few words of caution are in order here. First, also the experimental value of the ratio $R_c \equiv \Gamma(Z \rightarrow \bar{c}c)/\Gamma(Z \rightarrow \text{hadrons})$: $R_c^{exp} = 0.1598 \pm 0.0070$ [11] shows a disagreement (at the level of 1.7 standard deviations) with the SM prediction: $R_c^{SM} = 0.172$. Most disturbingly, this disagreement in R_c cannot be settled within the MSSM. These problems affecting R_b and R_c could be due to systematic errors in the experimental measurements, and might therefore disappear after the analysis of new data. However, it has to be pointed out that, even if R_c is constrained to the SM value, still the measured value of R_b shows a disagreement of 2.6 standard deviations with the SM value [11]. In the present note we focus our attention on the implications that the R_b problem would have for relic neutralinos, if the measured effect were real and could be accounted for, at least partially, by supersymmetric effects within the MSSM.

As was mentioned above, an important ingredient for a good χ^2 at small $\tan\beta$ is provided by a positive supersymmetric contribution to R_b , when the chargino is light. This feature is somewhat weakened [17] by the new LEP 1.5 lower bound on the chargino mass $m_{\chi^\pm} \geq 65$ GeV (if $m_{\chi^\pm} - m_\chi \gtrsim 10$ GeV, m_χ denotes the neutralino mass) [18]. However, this new limit does not modify appreciably the conclusions of the χ^2 analysis of Ref. [8], which we are going to use in the present note, since the lowest values of χ^2 at small $\tan\beta$ occur at larger values of the chargino mass, $m_{\chi^\pm} \simeq (75\text{--}90)$ GeV [10].

As far as large values of $\tan\beta$ are concerned, one should recall that significant constraints may potentially follow from the $Z \rightarrow b\bar{b}A$ process [19]. This argument was used in Ref. [20] to conclude that large values of $\tan\beta$ are disallowed by present experimental data. However, much larger statistics and/or more refined analyses of the LEP experimental data on four b -jets are still required, before solid conclusions on this point may be drawn (see also Ref. [10]). Here we consider the large- $\tan\beta$ sector of the parameter space as a region deserving much attention, because of the indications coming from the fit within the MSSM and in view of the very interesting perspectives that it offers for further investigation both at accelerators and with other experimental means (direct and indirect searches for relic neutralinos).

In the analysis presented in this note we take as representative values for case (i), i.e. small $\tan\beta$, and case (ii), i.e. large $\tan\beta$, the values: $\tan\beta = 1.4$ and $\tan\beta = 50$, respectively.

Now we briefly mention the main features of the best fit of Ref. [8], which are relevant to our subsequent discussion on the neutralino phenomenology [21]. Here all Z partial-widths and asymmetries at the Z pole are calculated and fitted using as free parameters the Higgs-mixing parameter μ , the ratio M_2/μ (M_2 is the SU(2) gaugino mass), the mass of the CP-odd Higgs boson m_A , the three soft scalar masses for the third family, the soft top trilinear coupling A_t and the strong gauge coupling α_s . The usual relation between U(1) and SU(2) gaugino masses $M_1 = \frac{5}{3} \tan^2\theta_W M_2$ is assumed. For details concerning the best-fit procedure we refer to [8,10]. Various values for the top quark mass were considered in the fit of Ref. [8]. In the present note we set it to $m_t = 170$ GeV.

For small $\tan\beta$ ($\tan\beta = 1.4$) the best fit ($\chi^2 \simeq 12$ –13) does not occur for the smallest possible value of the chargino mass, but rather for the range $m_{\chi^\pm} \simeq (75$ –90) GeV. In fact, for such chargino masses the ratio R_b obtains its largest value, $R_b \simeq 0.2180$, from the properties of the couplings occurring in the supersymmetric loop corrections to R_b , for one sign of μ , as explained in Ref. [10]. In the configurations providing the best fit ($\chi^2 \simeq 12$ –13), the lighter stop is very light indeed: $M_{\tilde{t}_2} \simeq 50$ GeV, the neutralino mass turns out to be constrained in the range $m_\chi \simeq (25$ –40) GeV, and the mass of the Higgs boson A is larger than about 200 GeV. If we consider all the configurations that satisfy the condition $\chi^2 \leq 16$, then the chargino and neutralino masses are in the ranges: 70 GeV $\lesssim m_{\chi^\pm} \lesssim 200$ GeV and 25 GeV $\lesssim m_\chi \lesssim 100$ GeV, respectively. The neutralino may have quite different compositions, from very pure gaugino-like to the other extreme of very pure higgsino-like. In the next section we will discuss the neutralino relic density. However, we anticipate here which are the modifications to the features of the best-fit previously discussed, when this best-fit analysis is implemented with the following constraints: (a) the neutralino is the Lightest Supersymmetric Particle (LSP), (b) the cosmological bound $\Omega h^2 \leq 1$ is satisfied. Condition (a) is imposed here by requiring the sfermion masses to be larger than the neutralino mass m_χ by at least 10%, i.e. $m_{\tilde{f}} \geq 1.1 m_\chi$. This requirement prevents some propagators in the elastic cross sections from becoming singular and also avoids possible complications due to co-annihilation [22]. It turns out that condition (b) is very effective, particularly in disallowing many configurations, since, at small $\tan\beta$, $\Omega_\chi h^2$ is usually very large. Thus, adding the two conditions (a) and (b) somewhat worsens the best-fit quality: the minimal χ^2 becomes 13.5 at $m_{\chi^\pm} \simeq 90$ GeV and $m_A \simeq 100$ GeV. In that region of the parameter space $m_\chi \simeq 40$ GeV. This last value is expected, because the cosmological bound is satisfied due to the very pronounced enhancement of the neutralino pair annihilation cross-section at the Z -pole ($m_\chi \simeq m_Z/2$). The region of the parameter space satisfying the condition $\chi^2 \leq 16$ has chargino and neutralino masses constrained in the ranges 65 GeV $\lesssim m_{\chi^\pm} \lesssim 110$ GeV and 25 GeV $\lesssim m_\chi \lesssim 80$ GeV.

Let us now turn to the large- $\tan\beta$ case ($\tan\beta = 50$). The best fit ($\chi^2 \simeq 12$ –13) occurs for the smallest possible values of the chargino mass and of the A -boson mass: $m_{\chi^\pm} \simeq 65$ GeV, $m_A \simeq 55$ GeV and for a light neutralino, $m_\chi \simeq 50$ GeV. This allows large values for R_b , up to $R_b = 0.2181$. Let us stress that the relevant chargino and neutralino compositions are mainly higgsino-like, as implied by the mass relation $m_\chi \simeq m_{\chi^\pm}$. If we consider all the configurations that satisfy the condition $\chi^2 \leq 16$, then the masses of chargino and neutralino are in the ranges: 65 GeV $\lesssim m_{\chi^\pm} \lesssim 250$ GeV, 50 GeV $\lesssim m_\chi \lesssim 190$ GeV. The cosmological condition $\Omega h^2 \leq 1$ is not effective in constraining the parameter space here, as is expected at large values of $\tan\beta$.

III. RELIC NEUTRALINOS

We now discuss the properties of the relic neutralinos, should the supersymmetric parameter space be the one singled out by the previously described χ^2 fit. In particular we discuss the neutralino relic abundance and detection rates for the direct search, where a relic neutralino may be detected by the energy released by its elastic scattering off a nucleus of an appropriate set-up [23–25].

Some words of caution are in order here, concerning the evaluation of the direct detection rates. It is well known that all the calculations for detection rates, in addition to the uncertainties due to the supersymmetric scheme, are also affected by many uncertainties in some astrophysical and cosmological properties. This is the case for the neutralino velocity distribution in the halo (assumed here to be Maxwellian with a r.m.s. velocity of $270 \pm 24 \text{ km} \cdot \text{s}^{-1}$ [26]), for its escape velocity ($v_{esc} = 650 \pm 200 \text{ km} \cdot \text{s}^{-1}$ [27]) and for the velocity of the Sun around the galactic centre ($v_{\odot} = 232 \pm 20 \text{ km} \cdot \text{s}^{-1}$ [26]). All these velocities are affected by large error bars, which in turn introduce significant uncertainties in the detection rates, especially for light neutralinos. Furthermore, an even more serious uncertainty concerns the value of the local (solar neighbourhood) dark matter density ρ_l . A recent determination of ρ_l , based on a flattened dark matter distribution and microlensing data, gives the range $\rho_l = 0.51_{-0.17}^{+0.21} \text{ GeV} \cdot \text{cm}^{-3}$ [28]. This introduces a central value significantly larger than previous determinations, for instance the one of Ref. [29]: $\rho_l = 0.3 \pm 0.1 \text{ GeV} \cdot \text{cm}^{-3}$, and then entails larger detection rates. Notice that the error bars affecting ρ_l are quite large.

Once a specific value for the local density of the *total* dark matter ρ_l is picked up, we are still confronted with the problem of assigning a value to the *neutralino* local density ρ_χ . Here, to determine the value of ρ_χ to be used in the detection rates, we adopt the following rescaling recipe [30]: for each point of the parameter space, we take into account the relevant value of the cosmological neutralino relic density. When $\Omega_\chi h^2$ is larger than a minimal $(\Omega h^2)_{min}$, compatible with observational data and with large-scale structure calculations, we simply put $\rho_\chi = \rho_l$. When $\Omega_\chi h^2$ turns out to be less than $(\Omega h^2)_{min}$, and then the neutralino may only provide a fractional contribution $\Omega_\chi h^2 / (\Omega h^2)_{min} \equiv \xi$ to Ωh^2 , we take $\rho_\chi = \rho_l \xi$. The value to be assigned to $(\Omega h^2)_{min}$ is somewhat arbitrary, in the range $0.03 \lesssim (\Omega h^2)_{min} \lesssim 0.2$.

In the present paper, as far as the values of the aforementioned astrophysical and cosmological parameters are concerned, we use the two sets of values reported in Table 1. Set I corresponds essentially to the central values for the various parameters, whereas set II corresponds to those values of the parameters, which, within the relevant allowed ranges, provide the lowest detection rates (once the supersymmetric variables are fixed). Set I is employed to discuss the average predicted rates, whereas set II is used to derive constraints on supersymmetric configurations, whenever the theoretical rates exceed the present experimental bounds.

As a further source of uncertainties affecting the detection rates, we finally mention the strength of the Higgs–nucleon coupling, which plays an important role in the neutralino–nucleus scattering. Here, for the relevant coupling we adopt the determination reported in Ref. [3].

Many experiments for direct detection of massive weak-interacting dark matter particles are under way, using various materials [25]. In the present note we consider detection rates for germanium detectors [31–35]. The most consistent procedure for comparing predicted

TABLE I. Values of the astrophysical and cosmological parameters relevant to direct detection rates. $V_{r.m.s.}$ denotes the root mean square velocity of the neutralino Maxwellian velocity distribution in the halo; V_{esc} is the neutralino escape velocity and V_{\odot} is the velocity of the Sun around the galactic centre; ρ_{loc} denotes the local dark matter density and $(\Omega h^2)_{min}$ the minimal value of Ωh^2 . The values of set I are the median values of the various parameters, the values of set II are the extreme values of the parameters which, within the physical ranges, provide the lowest estimates of the direct rates (once the supersymmetric parameters are fixed).

	Set I	Set II
$V_{r.m.s.}(\text{km} \cdot \text{s}^{-1})$	270	245
$V_{esc}(\text{km} \cdot \text{s}^{-1})$	650	450
$V_{\odot}(\text{km} \cdot \text{s}^{-1})$	232	212
$\rho_{loc}(\text{GeV} \cdot \text{cm}^{-3})$	0.5	0.2
$(\Omega h^2)_{min}$	0.1	0.2

detection rates with experimental data is to consider the differential rate dR_{direct}/dE_{ee} over the whole range of the electron-equivalent energy E_{ee} (or, alternatively, of the nuclear recoil energy). Here, to simplify the discussion, we present our results only in terms of an appropriate integrated rate R_{direct} . On the basis of the experimental spectra of Ref. [35] we derive, as the most stringent upper bound (at 90% C.L.) for light neutralinos ($20 \text{ GeV} \lesssim m_{\chi} \lesssim 50 \text{ GeV}$), the value [36]

$$\int_{6 \text{ keV}}^{8 \text{ keV}} dE_{ee} dR_{direct}^{exp}/dE_{ee} < 0.9 \text{ events}/(\text{kg} \cdot \text{day}). \quad (1)$$

In principle, for heavier neutralinos (m_{χ} larger than 50 GeV), which are expected to produce much flatter energy spectra, a more stringent bound (at 90% C.L., still using the data of Ref. [35]) is provided by

$$\int_{13 \text{ keV}}^{14 \text{ keV}} dE_{ee} dR_{direct}^{exp}/dE_{ee} < 0.1 \text{ events}/(\text{kg} \cdot \text{day}). \quad (2)$$

However, since the limit of Eq. (2) introduces only a marginal improvement over that of Eq. (1), for simplicity, in the present paper we only use the bound of Eq. (1), which we denote by R_{direct}^{exp} , and compare it with the relevant theoretical integrated rate $R_{direct} \equiv \int_{6 \text{ keV}}^{8 \text{ keV}} dE_{ee} dR_{direct}/dE_{ee}$.

IV. RESULTS AND CONCLUSIONS

Let us now turn to the presentation of our results, based on the supersymmetric configurations selected by the global fit to the electroweak data of Refs. [8,10]. We start from the small- $\tan\beta$ case. In Fig. 1 we show the neutralino relic abundance $\Omega_{\chi} h^2$ versus R_{direct} , for $\tan\beta = 1.4$. As was mentioned in Sect. 2, most of the configurations singled out by

the best-fit procedure at this value of $\tan\beta$ provide large values of $\Omega_\chi h^2$, in excess of the cosmological bound. The scatter plot shown in Fig. 1 displays only those supersymmetric configurations that satisfy the condition $\Omega h^2 \leq 1$. The rate R_{direct} reported in this figure was evaluated, using set I of Table 1. The vertical line corresponds to the experimental bound defined in Eq. (1).

We notice in Fig. 1 that many neutralino configurations provide a value for the relic abundance within the optimal range for Cold Dark Matter (CDM), $0.1 \lesssim \Omega_{CDM} h^2 \lesssim 0.3$, which is suggested by a number of observational data [37]. Many other supersymmetric compositions provide an even larger contribution to the neutralino relic abundance. As expected on general grounds, the predicted direct rates are all below the present experimental bound of Eq. (1). However, it is interesting to note that, by improving the experimental sensitivity of the direct experiments by about one order of magnitude (which appears to be within reach in the near future), one can start the investigation of a sizeable number of neutralino configurations (including many of cosmological interest).

Let us now turn to the large- $\tan\beta$ case. In Fig. 2 we display our results for the neutralino relic abundance versus the neutralino mass, as a scatter plot over all the configurations of the best-fit analysis with $\chi^2 \leq 16$, for $\tan\beta = 50$. In this scatter plot the points turn out to be grouped in some characteristic branches. This feature is due to the grid used in the χ^2 fit: along each branch the ratio $M_2/|\mu|$ has a fixed value, and each branch stops when m_{χ^\pm} reaches the maximal value considered in the fit: $m_{\chi^\pm} = 200$ GeV ($m_{\chi^\pm} = 250$ GeV for the value $M_2/|\mu| = 1$). The highest branch corresponds to the value $M_2/|\mu| = 0.5$ (gaugino dominance in the neutralino composition), the intermediate one belongs to the value $M_2/|\mu| = 1$ (large gaugino–higgsino mixing), and the lowest branch contains configurations with $M_2/|\mu| = 3, 10$ (higgsino dominance). The different nature of the neutralino compositions along the different branches explains the significant differences in their $\Omega_\chi h^2$ values. As expected, only gaugino-like neutralinos may have values of relic abundance in the desirable range $0.1 \lesssim \Omega_{CDM} h^2 \lesssim 0.3$. Actually, only very few configurations within the total best-fit sample fall into this range. However, it is rewarding that a large number of states provide a relic abundance of some cosmological interest, i.e. in the range $\Omega_\chi h^2 \gtrsim 0.025$.

Let us now discuss the event rates for direct detection of relic neutralinos. Figure 3 displays two scatter plots of the rate R_{direct} as a function of m_χ . The rate R_{direct} shown in section (a) was evaluated using set I in Table 1, the one shown in section (b) was evaluated using set II. In Fig. 3 configurations of different cosmological relevance are denoted by different symbols. The shape of the rate R_{direct} in these plots is reminiscent of the shape of the relic abundance displayed in Fig. 2, the reason being that the rescaling of the local neutralino density is very effective here. Of the two sets of points which branch off at $m_\chi \simeq 80$ GeV, the upper branch is mainly a combination of the configurations with $M_2/|\mu| = 0.5, 1, 3$, whereas the lower branch contains configurations with $M_2/|\mu| = 10$. In fact, the neutralino–nucleus cross section that enters in the detection rate has the effect of somewhat grouping together the configurations belonging to the three smallest values of $M_2/|\mu|$ and of further suppressing the rates for the purest higgsino states with $M_2/|\mu| = 10$. Of the two plots shown in Fig. 3, the one of section (a), which was obtained by using the values of set I for the astrophysical parameters, is indicative of what would be expected from direct detection, but suffers from uncertainties due to the large error bars affecting the various parameters. The plot of section (b) is the one which is relevant, when we address the question whether the

present experimental bound R_{direct}^{exp} already allows us to set some constraints on our sample of best-fit supersymmetric configurations. As a matter of fact, the scatter plot displayed in Fig. 3b represents a conservative estimate of the predicted rates. Thus we may conclude that the neutralino configurations, whose rates are above R_{direct}^{exp} in the plot of section (b), are excluded by the present experimental bound from direct detection experiments [38]. The number of the disallowed configurations is almost one tenth of the total number of about 3,000 configurations.

In Fig. 4 we display, in an R_b versus χ^2 plot, the frontier of the region that contains the whole sample of the best-fit configurations of Ref. [8] (this frontier is denoted by a solid line). The dashed curve delimits the region where are located those configurations of the original sample that are excluded by R_{direct}^{exp} on the basis of the results shown in Fig. 3b. However, we stress that the region inside the dashed curve is still populated by a large number of other allowed configurations.

Some noticeable properties emerge from our results:

- The configurations excluded by the present upper bound R_{direct}^{exp} are not located in the minimum of χ^2 (see Fig. 4). Actually, from details of our analysis which are not displayed in Fig. 4, it turns out that most of the excluded configurations are concentrated in the range $15 \lesssim \chi^2 \lesssim 16$. The configurations that give the minimal values of χ^2 have a very pure higgsino composition, and then provide a small detection rate. Therefore, the constraint introduced by R_{direct}^{exp} , although instrumental in limiting the parameter space, does not nevertheless modify the good quality of the fit significantly.
- Even a modest improvement in the sensitivity of the direct search experiments allows the exploration of a large number of neutralino configurations. This is clear from Fig. 3b, which shows that the R_{direct} vs. m_χ plot is highly populated around the line denoting the present upper bound R_{direct}^{exp} . For example, our calculations predict that, once the experimental sensitivity is improved by an order of magnitude with respect to the present one, more than 60% of the total number of the best-fit configurations can be explored. Some of them belong to the region of minimal χ^2 . Thus, the discovery potential of the direct search for relic neutralinos is quite remarkable.

Acknowledgements

We thank Stefan Pokorski, Piotr Chankowski and Nicolao Fornengo for interesting discussions. This work was supported in part by the Research Funds of the Ministero dell'Università e della Ricerca Scientifica e Tecnologica. A fellowship of the Università di Torino is gratefully acknowledged by G. Mignola. M. Olechowski would like to acknowledge the support of the Polish Committee of Scientific Research.

REFERENCES

- [1] M. Olechowski and S. Pokorski, *Phys. Lett.* **B344** (1965) 201.
- [2] N. Polonsky and A. Pomarol, *Phys. Rev. Lett.* **73** (1994) 2292; *Phys. Rev.* **D51** (1995) 6532; D. Matalliotakis and H. P. Nilles, *Nucl. Phys.* **B435** (1995) 115; A. Pomarol and S. Dimopoulos, *Nucl. Phys.* **B453** (1995) 83; H. Murayama, Berkeley preprint LBL-36962 (1995), hep-ph/9503392.
- [3] V. Berezhinsky, A. Bottino, J. Ellis, N. Fornengo, G. Mignola and S. Scopel, CERN preprint CERN-TH 95-206 (to appear in *Astroparticle Physics*), hep-ph/9508249.
- [4] V. Berezhinsky, A. Bottino, J. Ellis, N. Fornengo, G. Mignola and S. Scopel, CERN preprint CERN-TH 96-42, hep-ph/9603342.
- [5] J. Ellis, G.L. Fogli and E. Lisi, *Phys. Lett.* **286B** (1992) 85, *Nucl. Phys.* **B393** (1993) 3, *Phys. Lett.* **324B** (1994) 173 and **333B** (1994) 118; P. Langacker and M. Luo, *Phys. Rev.* **D44** (1991) 817; M. Carena and C.E.M. Wagner, *Nucl. Phys.* **B452** (1995) 45.
- [6] G. Altarelli, R. Barbieri and F. Caravaglios, *Phys. Lett.* **314B** (1993) 357.
- [7] D. Garcia and J. Solà, *Phys. Lett.* **B354** (1995) 335.
- [8] P. H. Chankowski and S. Pokorski, *Phys. Lett.* **366B** (1996) 188.
- [9] G.L. Kane, R.G. Stuart and J.D. Wells, *Phys. Lett.* **B354** (1995) 350.
- [10] P. H. Chankowski and S. Pokorski, preprint IFT-96/6 (hep-ph 9603310).
- [11] M.D. Hildreth, talk at the XXXI Rencontres de Moriond, March 1996.
- [12] A. Djouadi, G. Girardi, C. Verzegnassi, W. Hollik and F.M. Renard, *Nucl. Phys.* **B349** (1991) 48; M. Boulware and D. Finnell, *Phys. Rev.* **D44** (1991) 2054; A. Blondel and C. Verzegnassi, *Phys. Lett.* **B311** (1993) 346.
- [13] J. Erler and P. Langacker, *Phys. Rev.* **D52** (1995) 441.
- [14] L. Roszkowski and M. Shifman, *Phys. Rev.* **D53** (1996) 404.
- [15] M. Shifman, *Mod. Phys. Lett.* **A10** (1995) 605.
- [16] D. Garcia and J. Solà, *Phys. Lett.* **B357** (1995) 349.
- [17] J. Ellis, J.L. Lopez and D.V. Nanopoulos, CERN preprint CERN-TH/95-314, hep-ph/9512288.
- [18] L. Rolandi, H. Dijkstra, D. Strickland and G. Wilson, representing the ALEPH, DELPHI, L3 AND OPAL collaborations, Joint Seminar on the First Results from LEP 1.5, CERN, December 1995; ALEPH Collaboration, preprint CERN-PPE/96-10; OPAL Collaboration, preprint CERN-PPE/96-019 and CERN-PPE/96-020.
- [19] A. Djouadi, P. Zerwas and J. Zunft, *Phys. Lett.* **B259** (1991) 175.
- [20] J. Wells and G. Kane, *Phys. Rev. Lett.* **76** (1996) 869.
- [21] We thank Piotr Chankowski for providing us with the outputs of the χ^2 fit of Ref. [8], employed in our analysis.
- [22] K. Griest and D. Seckel, *Phys. Rev.* **D 43** (1991) 3191.
- [23] A. Bottino, V. de Alfaro, N. Fornengo, G. Mignola and S. Scopel, *Astroparticle Physics* **2** (1994) 77; A. Bottino, V. de Alfaro, N. Fornengo, G. Mignola, S. Scopel, and C. Bacci et al. (BRS Collaboration), *Phys. Lett.* **B295** (1992) 330. See also the review paper by G. Jungman, M. Kamionkowski and K. Griest, *Phys. Rep.* **267** (1996) 195, and references quoted therein.

- [24] L. Bergström and P. Gondolo, preprint OUTP-95-38P, hep-ph/9510252.
- [25] For reviews covering also the experimental aspects, see: J. R. Primack, D. Seckel and B. Sadoulet, *Annu. Rev. Nucl. Part. Sci.* **38** (1988) 751; P. F. Smith and J. D. Lewin, *Phys. Rep.* **187** (1990) 203; R. Bernabei, *Riv. N. Cim.* **18** (1995) N.5, and L. Mosca, invited talk at TAUP 95 (Toledo, September 1995) to appear in *Nucl. Phys. B* (Proc. Suppl.).
- [26] F. J. Kerr, D. Lynden-Bell, *Mon. Not. R. Astr. Soc.* **221** (1986) 1023.
- [27] P.J.T. Leonard and S. Tremaine, *Ap.J.* **353** (1990) 486.
- [28] E.I. Gates, G. Gyuk and M. Turner, Fermilab preprint FERMILAB-Pub-95/090-A, hep-ph/9505039.
- [29] R.A. Flores, *Phys. Lett.* **B215** (1988) 73.
- [30] T.K. Gaisser, G. Steigman and S. Tilav, *Phys. Rev.* **D34** (1986) 2206.
- [31] S. P. Ahlen et al., *Phys. Lett.* **B195** (1987) 603; D. O. Caldwell et al., *Phys. Rev. Lett.* **61** (1988) 510.
- [32] D. Reusser et al., *Phys. Lett.* **B255** (1991) 143.
- [33] M. Beck (Heidelberg–Moscow Collaboration), *Nucl. Phys. B* (Proc. Suppl.) **35** (1994) 150; M. Beck et al., *Phys. Lett.* **B336** (1994) 141.
- [34] E. Garcia et al., *Nucl. Phys. B* (Proc. Suppl.) **28A** (1992) 286; M. L. Sarsa et al., *Nucl. Phys. B* (Proc. Suppl.) **35** (1994) 154; E. Garcia et al., Proc. “The Dark Side of the Universe”, eds. R. Bernabei and C. Tao (World Scientific, Singapore 1994), p. 216.
- [35] A.K. Drukier et al., *Nucl. Phys. B*(Proc. Suppl.) **28A** (1992) 293; I. R. Sagdev, A. K. Drukier, D. J. Welsh, A. A. Klimenko, S. B. Osetrov, A. A. Smolnikov, *Nucl. Phys. B* (Proc. Suppl.) **35** (1994) 175.
- [36] We thank Angel Morales for providing us with the listings of the COSME [34] and TWIN [35] germanium spectra.
- [37] For a discussion of this point, see Ref. [4] and references quoted therein.
- [38] An analysis, along the general lines of the present paper, based on experimental bounds on up-going muon fluxes from the centre of the Earth and from the Sun (indirect neutralino detection) is in preparation.

Figure Captions

Figure 1 - Neutralino relic abundance $\Omega_\chi h^2$ versus R_{direct} , for $\tan\beta = 1.4$. This scatter plot displays only supersymmetric configurations that satisfy the condition $\Omega h^2 \leq 1$. The rate R_{direct} reported in this figure was evaluated, using set I of Table 1. The vertical line corresponds to the experimental bound given in Eq. (1).

Figure 2 - Neutralino relic abundance versus the neutralino mass, as a scatter plot over all the configurations of the best-fit analysis, for $\tan\beta = 50$.

Figure 3 - Scatter plots of the rate R_{direct} as a function of m_χ . The rate R_{direct} shown in section (a) has been evaluated using set I in Table 1, the rate R_{direct} shown in section (b) using set II. Configurations of different cosmological relevance are denoted by different symbols: configurations with a relic abundance $\Omega_\chi h^2 \geq 0.1$ are denoted by circles, those with a relic abundance in the range $0.025 \leq \Omega_\chi h^2 < 0.1$ are denoted by crosses, the other configurations by points.

Figure 4 - Plot of R_b versus χ^2 . The solid line delimits the region which contains the whole sample of the best-fit configurations of Ref. [8]. The dashed curve delimits the region where those configurations of the original best-fit sample excluded by R_{direct}^{exp} are located.

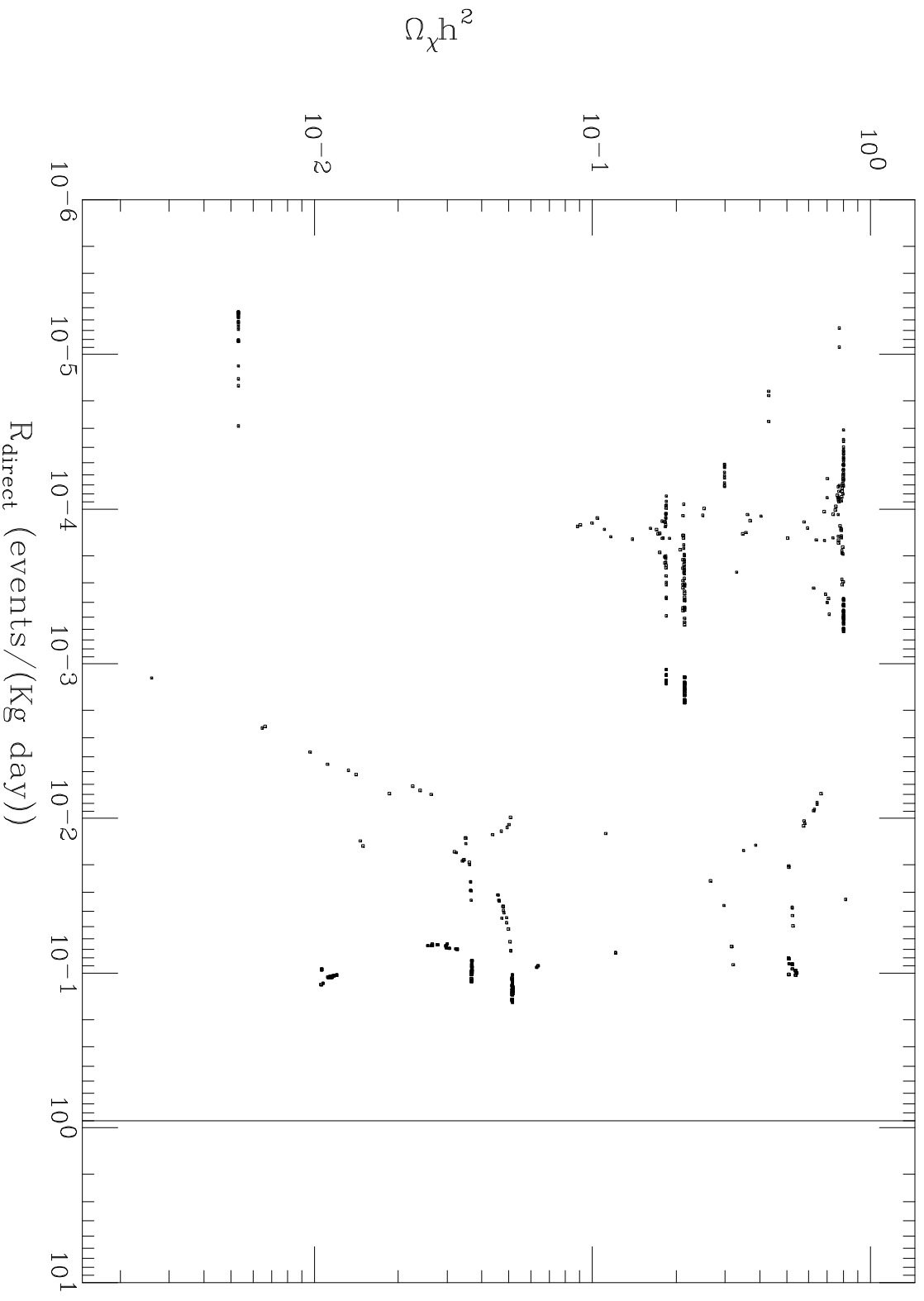


Figure 1

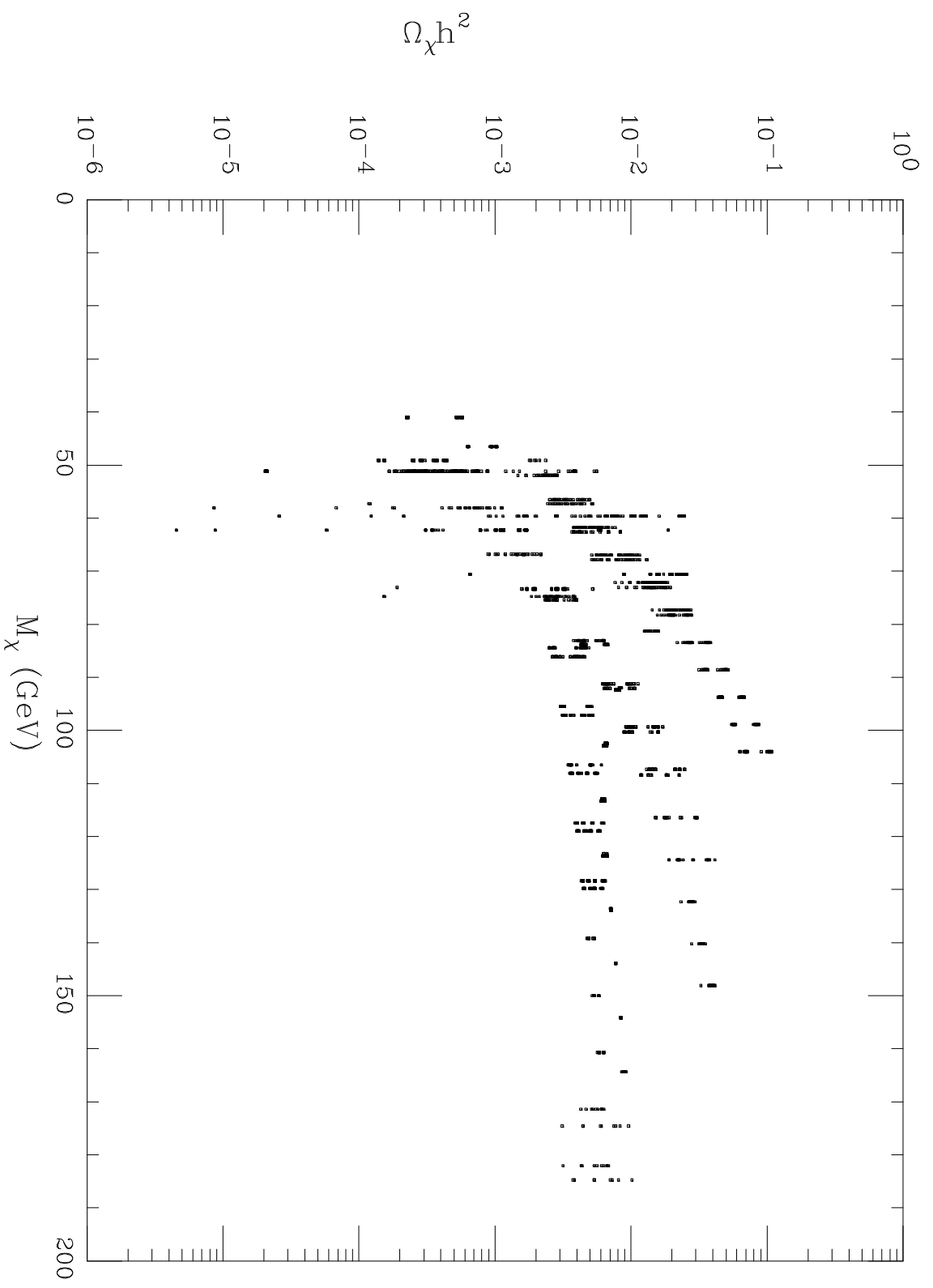


Figure 2

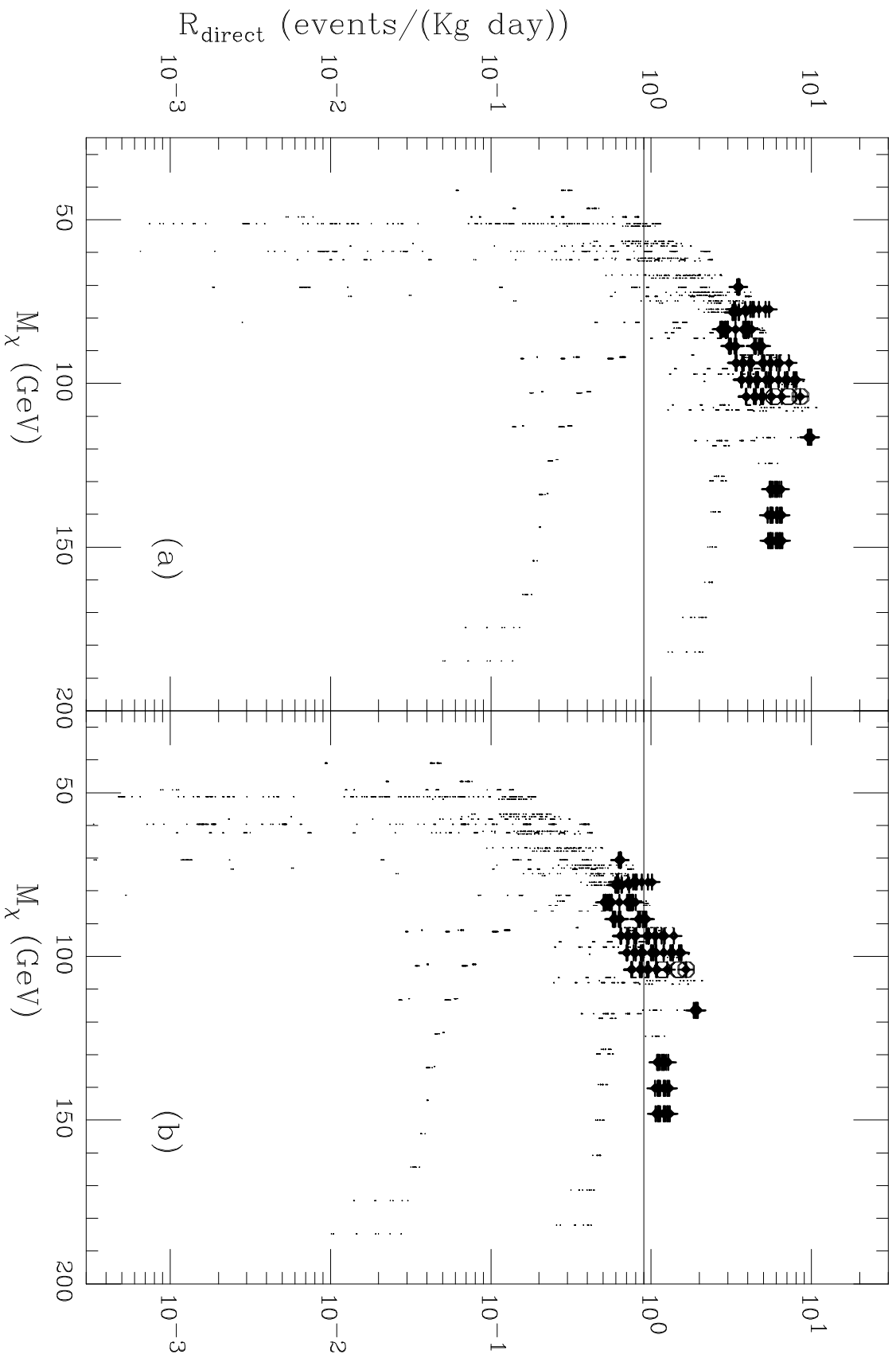


Figure 3

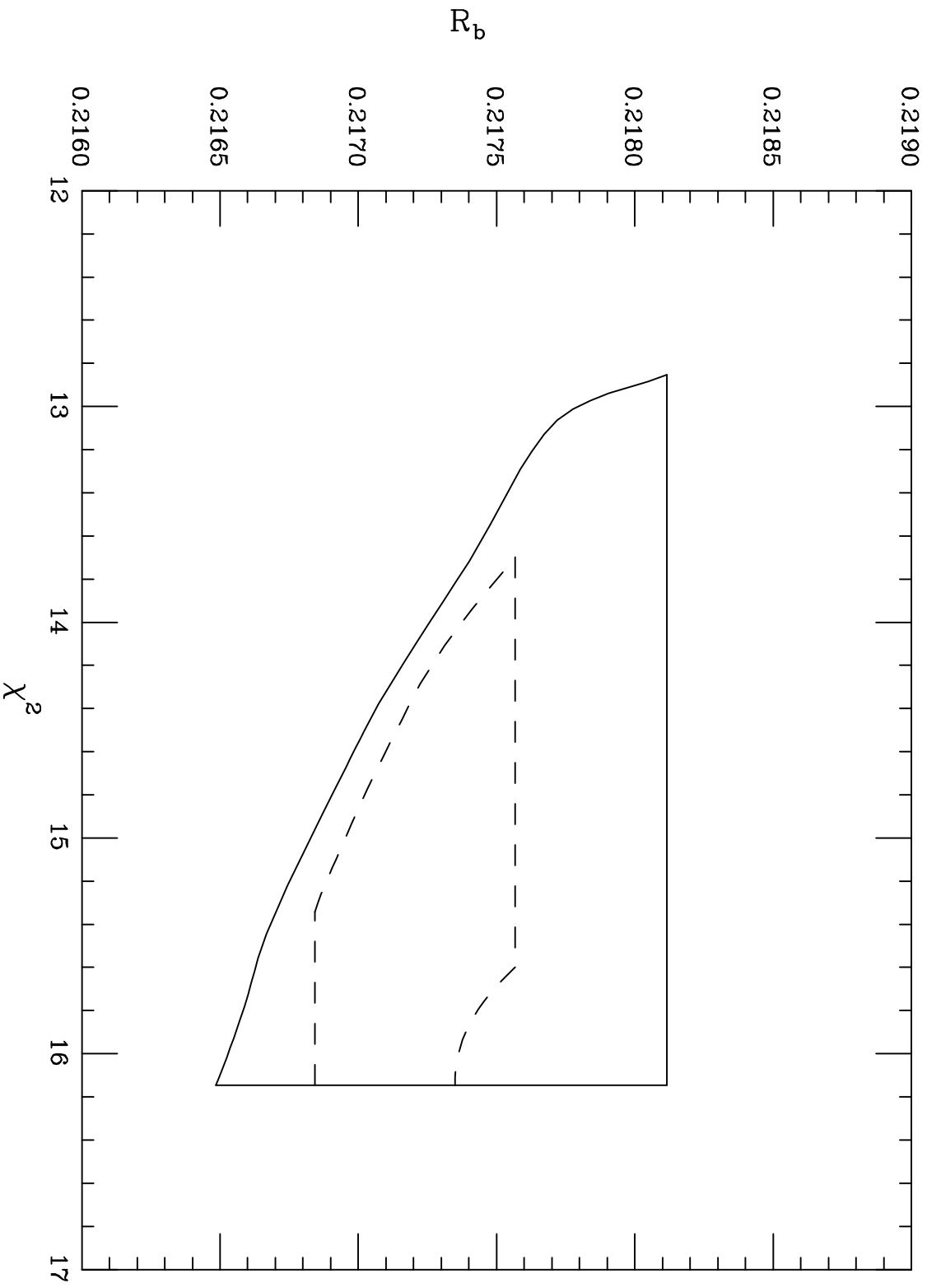


Figure 4